Folding of an mRNA Pseudoknot Required for Stop Codon Readthrough: Effects of Mono- and Divalent Ions on Stability†

Thomas C. Gluick,‡ Norma M. Wills,§ Raymond F. Gesteland,§ and David E. Draper*,‡

Department of Chemistry, Johns Hopkins University, Baltimore, Maryland 21218, and Howard Hughes Medical Institute and Department of Human Genetics, 6160 Eccles Genetics Building, University of Utah, Salt Lake City, Utah 84112

Received June 9, 1997; Revised Manuscript Received October 14, 1997⊗

ABSTRACT: Unfolding of an mRNA pseudoknot that induces ribosome suppression of the *gag* gene stop codon in Moloney murine leukemia virus has been studied by UV hyperchromicity and calorimetry. The pseudoknot melts in two steps, corresponding to its two helical stems. The total enthalpy of denaturation is ∼170 kcal/mol, approximately the value expected for the secondary structure. At low salt concentrations (<50 mM KCl) the unfolding transitions are not two-state, but they approach two-state behavior at higher salt concentrations. The structure is preferentially stabilized by smaller alkali metal ions ($Li^+ > Na^+ > K^+ > Rb^+ > Cs^+$) and by NH_4^+; the same preferences are exhibited by one of the stems in the context of a hairpin. Divalent metal ions are not required to fold the pseudoknot but do stabilize it further. To examine divalent ion effects over a wide concentration range, urea was used to lower the RNA unfolding temperature and was shown not to affect characteristics of the pseudoknot unfolding in other respects. The pseudoknot binds divalent ions somewhat more tightly than a hairpin but shows only weak selectivity for different size ions. It is suggested that a region of "intermediate" divalent ion binding affinity, in between highly ligated specific sites and purely delocalized ion binding in character, is created by the pseudoknot fold but that nonspecific, delocalized ion binding contributes at least half the free energy of pseudoknot stabilization by Mg^{2+}.

Functional RNAs are generally highly folded, compact structures whose stabilities are sensitive to the concentrations and types of ions present. Two basic types of ion interactions with RNAs may be imagined. The high negative charge of any nucleic acid is expected to accumulate an atmosphere of hydrated, delocalized cations that interact solely through long-range electrostatic forces (Anderson & Record, 1995). Closed shell alkali and alkaline earth metal ions interact with duplex DNA predominantly in this fashion (Manning, 1977; Bleam *et al*., 1980; Duguid *et al*., 1995), and the stabilization of duplex DNA by Na^+ and Mg^{2+} is due to such nonspecific interactions (Record, 1975). ["Non-specific" is used here in the way defined by Wyman and Gill (1990), to refer to electrostatically bound ions not following mass-action laws.] Since structures with higher charge densities have a larger fraction of their charge neutralized by ions, added salt should, in general, stabilize more compactly folded RNA conformations. In addition, an RNA structure may chelate an ion in a pocket of polar ligands (phosphate oxygens, base carbonyls or amines, and ribose hydroxyls), with ligands either binding directly to the ion or hydrogen bonding to ion-bound water. Such site-specific interactions may be selective for certain ions over others, as the size of the pocket, hydration of the ion, and number and types of ligands determine the ion binding affinity.

In a number of RNAs, site-bound ions are thought to be important contributors to tertiary structure stability. For instance, the tertiary structure of $tRNA_f^{Met}$ creates a single, high-affinity binding site for di- and trivalent ions at which the ion is partially dehydrated (Stein & Crothers, 1976a,b; Draper, 1985). The cooperative folding of group I introns is strongly linked to divalent ion binding (Laggerbauer *et al*., 1994; Zarrinkar & Williamson, 1994), and the crystal structure of an intron fragment shows a number of sites at which Mg^{2+} is bound (Cate *et al*., 1996). In two RNAs the selectivity of a structure for certain divalent ions has suggested the existence of specific sites; thus a complex pseudoknot is stabilized more effectively by Mg^{2+} than by other ions (Gluick *et al*., 1997), and a ribosomal RNA fragment also prefers Mg^{2+} (Laing *et al*., 1994; Bukhman & Draper, 1997). Monovalent ions may also interact at specific sites in nucleic acids. The best example is the preferential binding of K^+ in the channel created within a G quadruplex structure (Hud *et al*., 1996), and a requirement for NH_4^+ or K^+ in the formation of a ribosomal RNA tertiary structure has suggested the existence of specific monovalent ion binding site(s) (Wang *et al*., 1993). Given this variety of mono- and divalent ion interactions with RNA structures, it seems an important problem in RNA folding to establish the contributions of delocalized and site-bound ions to the overall stability of a folded RNA. In the past, thermodynamics of Mg^{2+} binding to tRNAs (Römer & Hach, 1975; Bina-Stein & Stein, 1976; Stein & Crothers, 1976a,b) and homopolymers (Krakauer, 1971, 1974) have been seriously studied, but, with the exception of ions required for ribozyme catalysis, there has been little additional quantitative work on ion−RNA interactions in recent years.

We previously used melting experiments to estimate the different affinities of Mg^{2+} ions for folded and unfolded forms of RNA hairpins (Laing *et al*., 1994). Only a small

† This work was supported by NIH Grant GM37005.

* To whom correspondence should be addressed: tel, 410-516-7448; fax, 410-516-8420; email, draper@jhunix.hcf.jhu.edu.

‡ Johns Hopkins University.

§ University of Utah.

⊗ Abstract published in *Advance ACS Abstracts,* December 1, 1997.

S0006-2960(97)01362-7 CCC: $14.00

preference of Mg^{2+} for nonspecific binding to duplex over single-stranded RNAs was needed to explain the observed stabilization. In the present study, we use this approach to look at ion interactions with a simple pseudoknot. In the most common H-type pseudoknot, hairpin loop nucleotides base pair with a sequence outside of the hairpin (ten Dam *et al*., 1992). As a result, three RNA strands are brought into close proximity at the junction of two helix segments. Folding of such a structure may be very sensitive to ion concentrations simply because of its high charge density; the junction of two helices may also create specific ion binding pockets. Thermodynamic studies of two pseudoknots have found that Mg^{2+} strongly promotes pseudoknot formation, and it has been suggested that a single Mg^{2+} binding site within the pseudoknot may explain this effect (Wyatt *et al*., 1990; Qiu *et al*., 1996).

The pseudoknot chosen for this study is from Moloney murine leukemia virus (MuLV)[1] mRNA (Figure 1A). Its function is to direct translating ribosomes to read through the *gag* gene stop codon and continue to translate *pol*. Folding of this sequence into a pseudoknot structure has been established by phylogenetic comparisons of viral RNAs, compensatory base mutations disrupting and restoring readthrough, and S1 nuclease mapping (Wills *et al*., 1991, 1994). The two stems are expected to be very stable, which we thought would be an advantage for studies of ion binding since the pseudoknot may form in the absence of Mg^{2+} and over a wide range of salt concentrations. The thermodynamics of folding this pseudoknot is also of functional interest, since read-through efficiency is potentially related to pseudoknot stability.

In the first part of this study we determine the thermodynamic stability of the pseudoknot in melting studies using UV hyperchromicity and calorimetry. We then examine the effects of different monovalent and divalent ions on the pseudoknot. The modest ion selectivity and ion binding affinities of the pseudoknot suggest the existence of a divalent ion binding region intermediate in character between completely delocalized and strongly chelated ions.

MATERIALS AND METHODS

Reagents and Buffers. All solutions were made in baked glassware to minimize ribonuclease contamination. Buffers and salt solutions were made from filtered and deionized water and treated with Chelex (Bio-Rad) to remove contaminating metal ions. Salts were generally reagent grade, except $BaCl_2$, $CaCl_2$, $MgCl_2$, and $SrCl_2$, which were Aldrich high purity grade. Buffers for melting experiments contained 5 mM sodium cacodylate, pH 7.0, plus the indicated concentrations of chloride salts. Some UV melting experiments contained 5 mM potassium phosphate (pH 7.0) instead of cacodylate; no differences were observed between experiments in the two buffers.

Plasmid Construction. Plasmids for T7 RNA polymerase transcription of RNAs H1 (hairpin 1) and G80 (pseudoknot) were made by ligating complementary deoxyoligonucleotides, containing a phage T7 promoter followed by the appropriate MuLV sequence, into pUC18 cut with *Bam*HI and *Eco*RI. Plasmid for H2 RNA (hairpin 2 and modified loop 2) was similarly constructed using the vector pTZ18U (U.S. Biochemicals) digested with *Eco*RI and *Hin*cII. pTZ18U contains a T7 promoter, and the transcription starts two nucleotides upstream of the *Eco*RI site. Consequently, H2 RNA contains a sequence GGGAAUUC (see Figure 1 or 2) at its 5′-end that is unrelated to MuLV sequences. DNA sequences of the inserts were verified by dideoxy sequencing.

RNA Structure Mapping. DNA templates were linearized with either *Eco*RV (pUC18 derivatives) or *Hin*cII (pTZ18U derivatives) prior to run-off transcription using T7 RNA polymerase (Promega) as directed by the manufacturer. Reactions were terminated by addition of phenol, precipitated with ethanol, resuspended in loading buffer (8 M urea, 2× TBE), and analyzed by electrophoresis through a 12% polyacrylamide−8 M urea gel in 1× TBE. RNAs were visualized by UV shadowing, excised and electroeluted in 0.5× TBE, and precipitated with ethanol. (1× TBE is 0.1 M Tris, 0.1 M boric acid, and 0.5 M Na_2EDTA.)

RNAs were dephosphorylated by calf intestinal alkaline phosphatase (New England Biolabs). After phenol extraction and ethanol precipitation, 100 pmol of each RNA was radiolabeled at the 5′-end using phage T4 polynucleotide kinase (New England BioLabs) and [^{32}P]-ATP (New England Nuclear). Nucleases S_1, T_1, and V_1 were obtained from Pharmacia. Reaction conditions were modified from those described in Larsen *et al*. (1997). The digestion buffer for T_1 and V_1 contained 50 mM sodium cacodylate, pH 7.5, and 20 mM magnesium acetate; for S_1, the digestion buffer was supplemented with 1 mM zinc acetate. Optimum enzyme concentrations for each RNA were determined by titration. Each reaction contained 100 000−200 000 cpm of labeled RNA and 1 μg of yeast tRNA. RNAs were preincubated at 37 °C prior to the addition of enzyme. Reactions were incubated further for 7−8 min and then stopped by addition of phenol. RNAs were recovered by precipitation with ethanol. The precipitate was resuspended in 8 M urea with 2× TBE loading buffer. Approximately 30 000 cpm of each reaction was loaded onto a 50 cm 12%−8 M urea polyacrylamide gel and run using standard conditions (Larsen *et al*., 1997). In addition to the enzymatic reactions done under native conditions, RNA ladders were generated by alkaline hydrolysis and by T_1 digestion under denaturing conditions.

Preparation of RNAs for Melting Experiments. RNAs were prepared by run-off transcription of plasmid DNA cut with restriction nuclease, as previously described (Gluick & Draper, 1994). The reaction mixture was filtered through a 0.45 μm filter, spin dialyzed (Centricon 10 or 3), and subsequently purified by denaturing preparative gel electrophoresis followed by electroelution in an Elutrap (Schleicher & Schuell). RNAs were precipitated with ethanol and stored as concentrated stocks in 1 mM MOPS, pH 7.0.

RNAs were prepared for UV melting experiments by diluting an aliquot of stock solution to 1 mL with the desired buffer. A modified Perkin-Elmer Lambda 4B spectrophotometer was used to collect absorbance data as a function of temperature and has been described (Laing & Draper, 1994). Heating rates were 0.5°/min; cooling curves were also taken to check for reversibility. RNAs (~1 mg/mL) were prepared for calorimetry by 2× dialysis against 2 L of the desired buffer solution. An extinction coefficient of 41.4 $\mu g/A_{260}$ unit was used. Calorimetry was done in a nano differential scanning calorimeter (Calorimetry Sciences Corp.) scanned at 1°/min. CSC software was used for preliminary data

[1] Abbreviations: MuLV, Moloney murine leukemia virus; TBE, Tris−borate−EDTA buffer.

analysis. Excess heat capacity curves of both buffer and sample were obtained.

Analysis of UV Melting Profiles and Excess Heat Capacity Curves. In all the melting data presented here, two or more unfolding events take place. Complications that arise in extracting thermodynamic parameters when multiple unfolding steps are present have been discussed elsewhere (Draper & Gluick, 1995). Briefly, each transition has associated with it a melting temperature (T_m), van't Hoff enthalpy (ΔH), and either a percent hyperchromicity (ΔA) in the case of UV melting data or a change in heat capacity (ΔC_p) for calorimetry data. Unique determination of all three parameters for each transition may not be possible if transitions are closely spaced (in hyperchromicity data) or if the overall ΔC_p of unfolding is significant (i.e., the calorimetry baseline is uncertain). As a way around this problem, we developed a computer program that simultaneously considers any combination of two or three melting data sets, including UV melting data collected at two different wavelengths (280 and 260 nm) and calorimetry data. T_m and ΔH for any one transition are constrained to remain the same among all data sets under consideration, while ΔA_{260}, ΔA_{280}, and ΔC_p apply to an individual data set. A sequential unfolding pathway, in which one unfolding step must occur before the next, is assumed; this model is more generally applicable than independent transitions (Draper & Gluick, 1995). Low- and high-temperature baselines are fixed by the user for both UV and calorimetry data sets. The program is an extension of an earlier program used to fit UV hyperchromicity data (Laing & Draper, 1994; Draper & Gluick, 1995).

For analysis of G80 RNA calorimetry experiments, data were also fit to sequential transitions in which each unfolding could deviate from two-state behavior by a factor y representing the ratio of calorimetric and van't Hoff enthalpies; for a single unfolding step the excess heat capacity is given by

$$C_p = \frac{y\Delta H^2 K}{(1+K)^2 RT^2} \quad (1)$$

Analysis of Ion Binding. A general equation for the change in T_m of a two-state RNA transition when ligands bind to multiple sites on either folded or unfolded RNA forms has been derived (Laing *et al*., 1994). For the analysis of divalent ion binding in the present study, we have assumed that each phosphate is a potential binding site and that one ion interacts with two phosphates; this nearest neighbor exclusion model has been used to analyze Mg^{2+} binding to homopolymers (Record *et al*., 1976). The equation used to fit the data is

$$\frac{1}{T_m} = \frac{1}{T_t} - \frac{R}{\Delta H_t}\ln\left(\frac{0.5 + 0.5(1+4K_fL)^{1/2}}{0.5 + 0.5(1+4K_uL)^{1/2}}\right)^m \quad (2)$$

where L is the free ligand (Mg^{2+}) concentration; K_f and K_u are ligand affinities for folded and unfolded forms of the RNA, respectively; ΔH_t and T_t are the enthalpy and melting temperature of the RNA in the absence of ligand; and m is the number of phosphates involved in the unfolding reaction (Laing *et al*., 1994). The numerator and denominator of the log term are binding polynomials for excluded site interactions, as given by Hill (1957). A derivative of the polynomial can be used with the association constants given in Table 3 to calculate the extent of ion binding, ν, at a given Mg^{2+} concentration (Wyman & Gill, 1990):

$$\nu = \frac{\partial \ln(0.5 + 0.5(1+4KL)^{1/2})^m}{\partial \ln L} = \frac{2mKL}{(1+4KL)^{1/2} + (1+4KL)} \quad (3)$$

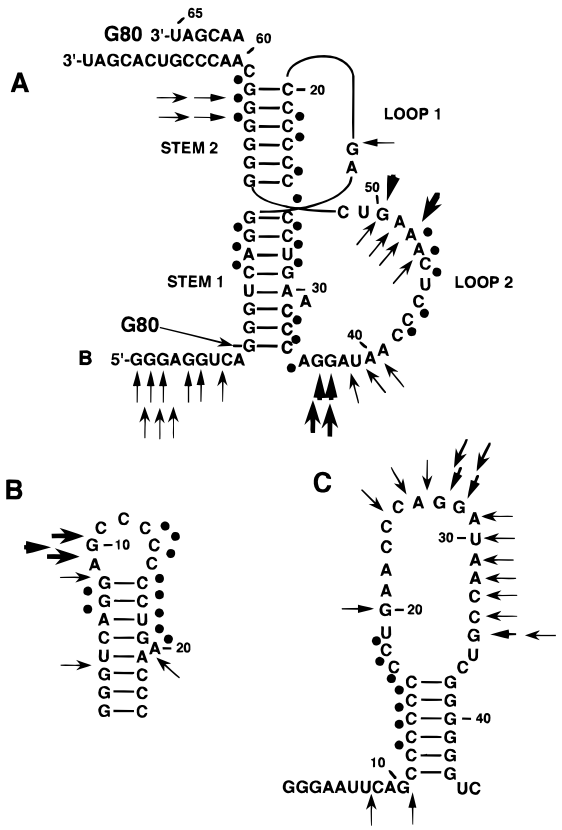

FIGURE 1: Structures of the MuLV pseudoknot and its component hairpins. (A) G80 RNA. The sequence shown was used in structure mapping experiments (Figure 2); the shorter termini labeled G80 correspond to the RNA used for melting experiments. (B) H1 RNA. (C) H2 RNA. Structure mapping results are indicated by (●) V_1 cleavage, (square arrowhead), T_1 cleavage, and (angular arrowhead), S_1 cleavage. Thicker symbols indicate more rapid cutting.

RESULTS

Secondary Structure of G80 Pseudoknot RNA and Its Component Hairpins. The sequences and secondary structures of the RNAs used in this study are shown in Figure 1. G80 RNA is a fragment of MuLV mRNA from the 5′-end of the *pol* gene and contains a pseudoknot essential for read-through of the upstream *gag* gene termination codon (Wills *et al*., 1991). Several mRNA fragments with different 5′- and 3′-termini were examined in preliminary melting experiments; some of these appeared conformationally heterogeneous or otherwise unsuitable for detailed study. G80 RNA is the shortest sequence that contains all of the nucleotides essential for wild-type levels of read-through (Wills *et al*., 1994).

The G80 RNA sequence folds into a pseudoknot in the context of functional mRNAs (Wills *et al*., 1991, 1994). To make sure that G80 RNA itself also adopts a pseudoknot structure, enzymatic probes were used to map its secondary structure: T_1 and S_1 nucleases are specific for single-stranded

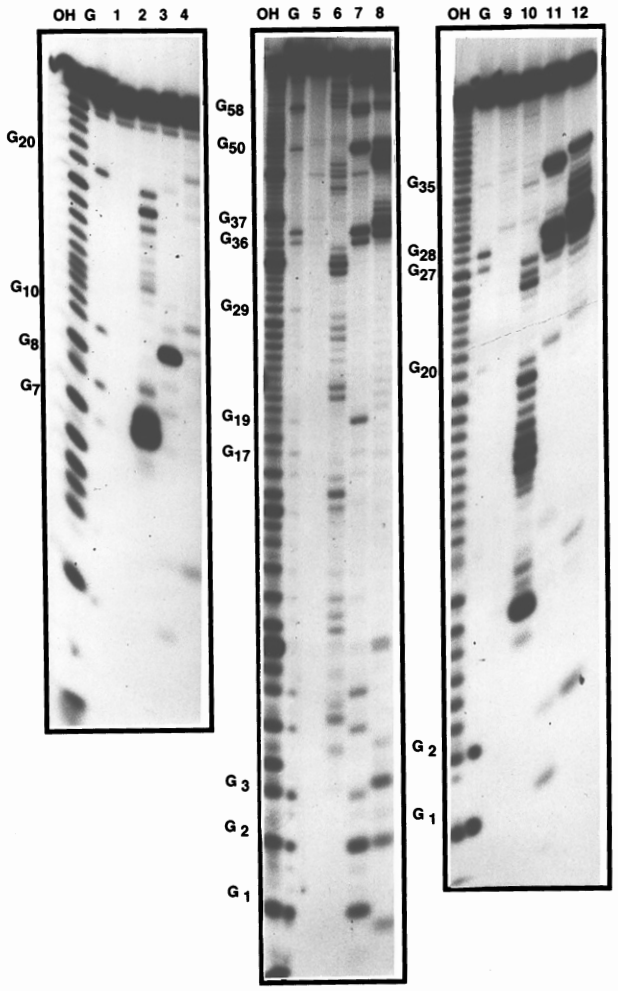

FIGURE 2: Enzymatic probing of MuLV pseudoknot and H1 and H2 RNAs. Lanes: OH, alkaline cleavage; G, T_1 RNase sequencing ladder; 1, 5, and 9, control lanes (no enzyme added); 2, 6, and 10, V_1 RNase (0.04 unit); 3, 7, and 11, T_1 RNase (0.05 unit); 4, 8, and 12, S_1 nuclease (5 unit).

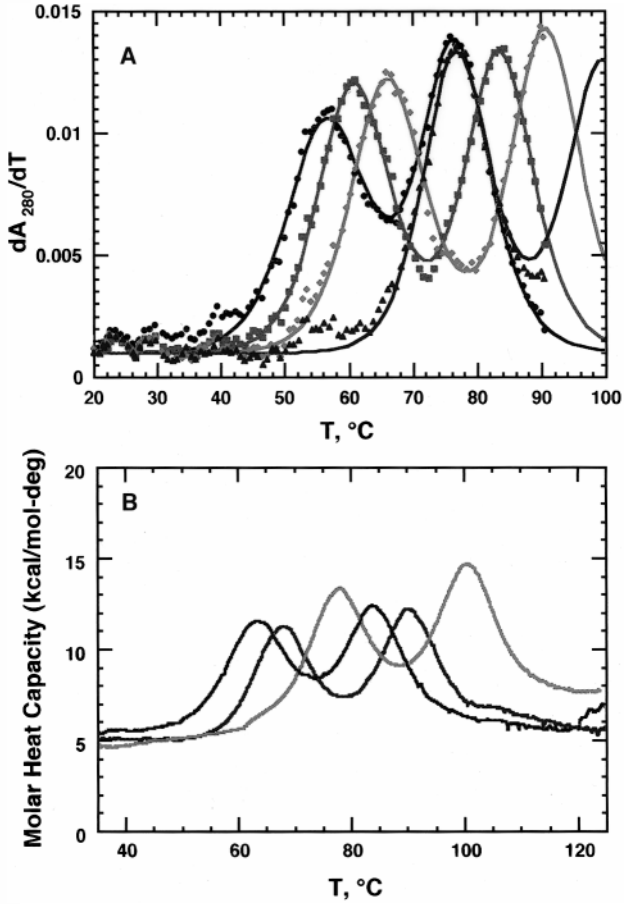

FIGURE 3: Unfolding of G80 RNA. (A) UV melting profiles obtained at 280 nm (points) with fitted curves (solid lines) for G80 RNA in buffer with 50 mM KCl (black), 100 mM KCl (green), 200 mM KCl (red), and 1000 mM KCl (blue). The parameters for the fits are listed in Table 1. (B) Excess heat capacity curves measured for G80 RNA in buffer with 100 mM KCl (black), 200 mM KCl (red), and 1000 mM KCl (blue).

nucleotides; V_1 nuclease cleaves RNA whose backbone is in an approximately helical conformation (Lowman & Draper, 1986). At the same time, two additional RNAs that duplicate either stem of the pseudoknot, H1 and H2, were synthesized and studied. The results of the probing experiments for G80 RNA are shown in Figure 2, and an interpretation of the results for all three RNAs is given in Figure 1.

The structure mapping results are consistent with G80 RNA adopting a pseudoknot conformation approximately as predicted and with H1 and H2 forming the expected hairpins. (Structure mapping with T_1 and S_1 nucleases in the absence of Mg^{2+} gave approximately the same results as shown in Figure 2.) One ambiguity that arises is the base pair G17-C26 at the junction between the two stems. G17 is weakly cut by T_1 and S_1 nucleases but not by V_1 nuclease, suggesting that it is single stranded at least part of the time. C26 is not cleaved by S_1 nuclease and is recognized by V_1 nuclease; it must be at least stacked upon stem 1 or stem 2, if not actually base paired. The analogous C in H1 RNA is also cut by V_1 nuclease, suggesting that the C can stack without base pairing. Another pseudoknot, from MMTV, also shows weak single-strand-specific cuts at a junction nucleotide, and an NMR study suggests that the stems are not coaxially stacked (Chen *et al*., 1996).

Loop 1 nucleotides A18 and G19 are readily cleaved by single-strand-specific reagents in H1 RNA but are less accessible in the intact pseudoknot, as might be expected for a short loop spanning a helix groove. In stem 2, G56 and G57 are recognized by single- and double-stranded specific nucleases, suggesting some fraying at the end of the helix. The larger loop 2 must be weakly structured in some way, since C42−A48 are cut by V_1 nuclease or S_1 nuclease. Perhaps the loop adopts a stacked conformation parallel to stem 1. At approximately the same loop 2 region as the V_1-sensitive nucleotides are six nucleotides (C44−A49) that are dispensable for read-through activity (Wills *et al*., 1994); these have been deleted in H2 RNA. The same deletion in G80 RNA has little effect on its melting behavior (data not shown).

Unfolding of G80 RNA. Melting of G80 RNA, as followed by either UV hyperchromicity or calorimetry, takes place in two distinct transitions over a range of monovalent and divalent ion concentrations (10−1000 mM KCl with between 0 and 20 mM $MgCl_2$; see example melts in Figure 3). Calorimetry experiments used G80 RNA concentrations nearly 100-fold higher than those in the UV experiments. Coincidence of the apparent T_ms between the two experiments carried out in the same buffer indicates that the unfolding steps are unimolecular. The resolution of G80 RNA unfolding into two major unfolding steps contrasts with

Table 1: Thermodynamic Parameters for G80 RNA Unfolding[a]

	van't Hoff analysis				UV/cal analysis				non-two-state		
buffer[b]	ΔH_{vH}	T_m	ΔA_{280}	ΔA_{260}	ΔH_{vH}	T_m	ΔA_{280}	ΔA_{260}	ΔH_{vH}	T_m	$\Delta H_{vH}/\Delta H_{cal}$
PK_{25}											
trans 1	27.2	38.6	0.063	0.0110							
trans 2	50.5	53.8	0.108	0.0540							
trans 3	59.7	68.7	0.197	0.0334							
PK_{50}											
trans 1	51.4	56.8	0.159	0.0656							
trans 2	68.4	76.8	0.176	0.0252							
PK_{100}											
trans 1	59.1	61.0	0.165	0.0664	65.3	62.6	0.112	0.0505	59.9	63.6	0.68
trans 2					36.3	73.5	0.044	0.0159			
trans 3	71.9	83.6	0.172	0.0236	66.1	84.0	0.110	0.0108	68.2	84.7	0.87
trans 4					29.0	95.0	0.040	0.0250	26	95	0.9
PK_{200}											
trans 1	59.8	66.2	0.172	0.0657	65.5	68.3	0.124	0.0501	66.9	67.8	0.83
trans 2					27.3	76.6	0.0213	0.0058			
trans 3	72.8	90.8	0.191	0.0336	71.1	89.9	0.129	0.0198	76.3	90.1	0.98
trans 4					35.2	104	0.0183	0.0023	30	104	1
PK_{1000}											
trans 1	70.2	76.9	0.171	0.0641	71.9	77.3	0.120	0.0449	74.9	77.8	0.83
trans 2					29.2	87.5	0.0285	0.0179			
trans 3	nd	nd	nd	nd	73.2	100.	0.13[c]	0.02[c]	77.3	100	0.91
trans 4					29.3	109	0.02[c]	0.01[c]	30	109	

[a] Simultaneous fitting of sequential transitions to sets of UV and calorimetry melting data was done as described in Materials and Methods. The combinations of data sets used were as follows: van't Hoff analysis, two transitions fit to UV melting profiles taken at 260 and 280 nm; UV/cal analysis, four transitions fit to two UV melting profiles and to calorimetry data; non-two-state analysis, two non-two-state transitions fit to calorimetry data alone. The fitting parameters are described in Materials and Methods; units are kcal/mol for ΔH and degrees Celsius for T_m. Approximate errors are T_m, ±0.7 deg, and ΔH and ΔA, ±15%. nd, transition temperature too high for parameters to be determined. [b] Buffers are 5 mM potassium phosphate plus the millimolar concentration of KCl indicated by the subscript. [c] Values were fixed to these values for fitting, since UV data do not extend past ~90 °C.

some other pseudoknots that melt in a single major transition (Wyatt *et al*., 1990; Qiu *et al*., 1996).

Both G80 RNA unfolding transitions show a larger percentage hyperchromicity at 280 nm than at 260 nm, which is a consequence of the G-C richness of the two pseudoknot stems. Melting profiles were fit to sequential two-state transitions (Draper & Gluick, 1995), simultaneously considering both 260 and 280 nm data sets. By constraining the transition melting temperatures and enthalpies to be identical between data sets collected at two different wavelengths, closely spaced unfolding transitions are more reliably identified than possible with hyperchromicity data collected at only one wavelength (see Materials and Methods). At salt concentrations above ~50 mM, the ratio of hyperchromicities at 260 and 280 nm remains constant through each of the melting profile peaks, and the data are fit very well by two transitions. At the lowest salt concentration the first peak broadens and its apparent T_m is different at 260 and 280 nm; this melting profile required inclusion of a third transition. The resulting parameters are listed in Table 1. The van't Hoff enthalpy of the first unfolding step increases from 51 to 70 kcal/mol as the salt concentration is raised from 50 to 1000 mM, even though it is fit by a single two-state transition over this range. Since RNA unfolding enthalpies are not strongly salt dependent (Breslauer *et al*., 1975; Williams *et al*., 1989), this suggests that the first unfolding step is only approximately two-state at lower salt concentrations.

For a further check of the applicability of two-state behavior to G80 RNA unfolding, calorimetry experiments were carried out; excess heat capacity curves at three salt concentrations are shown in Figure 3B. Because G80 RNA is very stable at the salt concentrations needed to induce approximately two-state behavior, it was necessary to extend the temperature range above 100 °C to obtain high-temperature baselines in these experiments. However, only ~50% of the RNA is recovered intact after scanning to 125 °C. In control experiments, it was found that intact G80 RNA can be recovered after incubation at 90 °C. We therefore presume that the broad transition at 100−115 °C, apparent in the experiments with 100 and 200 mM KCl, is principally due to RNA hydrolysis. As an approximate way to factor out this hydrolysis, we included an additional two-state transition at high temperatures (~95 °C) in the data analysis.

It is not possible to fit the calorimetry data with the parameters derived from the van't Hoff analysis of UV melting data, as the total calorimetric enthalpy of unfolding (after factoring out high-temperature hydrolysis) is 25−30 kcal/mol larger than the sum of the van't Hoff enthalpies of the two transitions (Table 1). Two alternatives exist. One is to assume the existence of a third transition, not apparent in the UV melting profiles. At any one salt concentration, the excess heat capacity curve and UV melting profiles at 260 and 280 nm could be simultaneously fit by three two-state transitions (in addition to the transition attributed to RNA hydrolysis); an example fit is shown in Figure 4A. The fitted parameters are listed in Table 1 (UV/cal analysis); the total enthalpy of unfolding is approximately the same at all three salt concentrations (164−174 kcal/mol). The "extra" transition appears in between the two larger enthalpy transitions.

The alternative way to account for the calorimetry data is to assume that the two unfolding transitions are not accurately described by a two-state model. Two transitions with ratios of van't Hoff to calorimetric enthalpies between ~0.7 and 1.0 give excellent fits to the data (Figure 4B). The approximation of two-state unfolding improves at higher salt

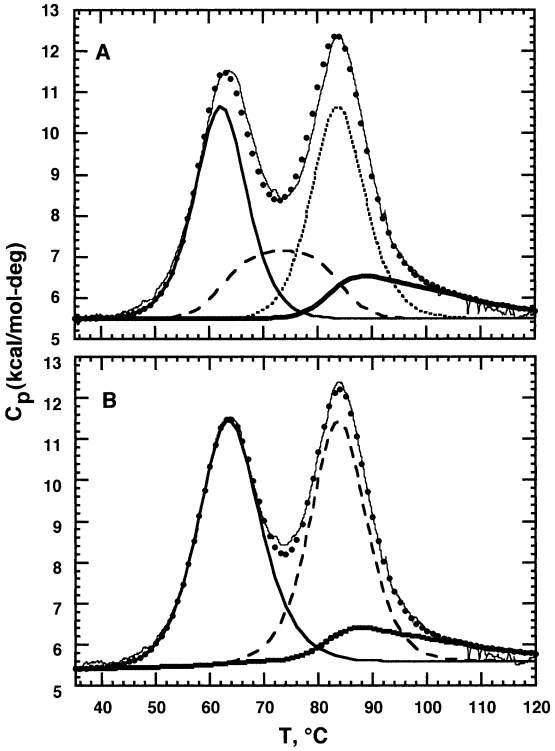

FIGURE 4: Deconvolution of G80 RNA calorimetry data. Parameters are given in Table 1. (A) Four two-state, sequential transitions. Curves: experimental heat capacity (thin —), fitted total heat capacity (●), transition 1 (medium —), transition 2 (— —), transition 3 (---), and transition 4 (thick —). (B) Three sequential transitions, with the first two transitions non-two-state. Curves: experimental heat capacity (thin —), fitted total heat capacity (●), transition 1 (medium —), transition 2 (— —), and transition 3 (thick —).

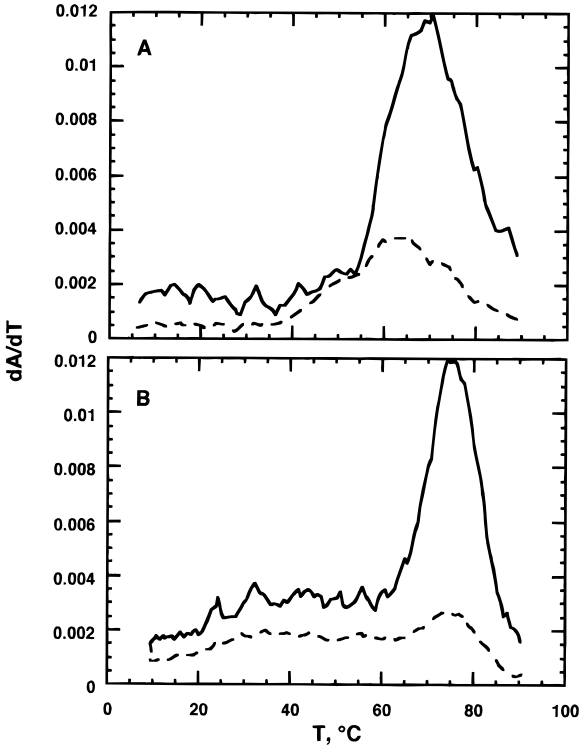

FIGURE 5: Melting profiles of H1 and H2 RNA in buffer with 50 mM KCl. (A) H1 RNA: 280 nm (—) and 260 nm (— —). (B) H2 RNA: 280 nm (—) and 260 nm (— —).

concentrations. The total enthalpy of unfolding is of course similar to that obtained with three two-state transitions; the difference between the two deconvolutions in Figure 4 is the presence or absence of a cooperatively unfolding structure of ~30 kcal/mol. The two larger enthalpy transitions presumably represent melting of the two stems (see analysis of individual hairpins below).

The minimum enthalpy expected for G80 RNA unfolding can be estimated by adding the nearest neighbor base stacking enthalpies for the two helical stems shown in Figure 1 (Turner *et al*., 1988); the value is 139 kcal/mol. This is approximately the van't Hoff enthalpy calculated from analysis of the UV melting curves alone at higher salt concentrations (Table 1). Stacking of 3′-nucleotides on the two stems and coaxial stacking between the two pseudoknot stems could add 24 kcal/mol to the unfolding enthalpy (Turner *et al*., 1988). The total enthalpy found in the calorimetry experiments (160−170 kcal/mol) therefore corresponds quite reasonably to the enthalpy expected for unfolding of the pseudoknot secondary structure alone. This correspondence between predicted and measured calorimetric enthalpy of unfolding, together with the deviations from two-state behavior already noted for the first unfolding transition, suggest that the pseudoknot unfolding is better described by two unfolding steps that deviate from two-state behavior.

To summarize our conclusions from the UV and calorimetry melting experiments, G80 RNA unfolds in two major steps. The first unfolding deviates strongly from two-state behavior at KCl concentrations less than 50 mM. At higher salt concentrations, van't Hoff analysis still underestimates the total enthalpy of unfolding; the simplest model assumes that unfolding occurs in only two, approximately two-state, steps. For the studies of ion−pseudoknot interactions described below, we use a van't Hoff analysis of UV melting data. The deviation from two-state behavior introduces only a small error into our measurements.

Unfolding of Hairpins H1 and H2. To see if the two unfolding transitions of G80 RNA could be identified with the individual stems of the pseudoknot, we examined the melting behavior of hairpins H1 and H2 (Figure 1). Melting profiles of these RNAs in 100 mM KCl buffer are shown in Figure 5. We argue from a comparison of thermodynamic parameters between the hairpins and G80 RNA that stem 1 melts first, followed by stem 2.

The hyperchromicity of melting H2 RNA is proportioned into a broad, nearly indistinct low-temperature transition and a sharp, high-temperature transition (Figure 5B). Parameters from two-wavelength analysis of these melting profiles at KCl concentrations between 25 and 1000 mM are given in Table 2. All of the melting profiles could be fit with two transitions. The broad transition has an apparent enthalpy that increases from 11 to 25 kcal/mol over this range of salt concentrations, while its T_m increases from 41 to only 62 °C. This ill-defined transition probably corresponds to unfolding of a mixture of weak structures within the large hairpin loop. The second transition has a large van't Hoff enthalpy, varying between 57 kcal/mol at 25 mM KCl and 69 kcal/mol at 200 mM KCl, and the associated hyperchromicity at 260 nm is only 13−17% of that seen at 280 nm. A larger 280 nm hyperchromicity is expected for the melting of the entirely G-C stem (Puglisi & Tinoco, 1989). There is a striking correspondence between the salt dependences of the second transition T_ms of H2 and G80 RNAs (Figure 6). This correspondence suggests that stem 2 is the last

Table 2: Thermodynamic Parameters for H1 and H2 RNA Unfolding[a]

	H1 RNA				H2 RNA			
buffer[b]	ΔH_{vH}	T_m	A_{280}	A_{260}	ΔH_{vH}	T_m	A_{280}	A_{260}
PK_{25}								
trans 1	30.1	53.5	0.0390	0.0819	11.5	40.7	0.152	0.0979
trans 2	34.6	64.1	0.284	0.0589	57.3	67.2	0.141	0.0180
PK_{50}								
trans 1	28.3	59.2	0.0455	0.0820	13.4	46.0	0.144	0.0906
trans 2	35.7	68.4	0.273	0.0537	64.7	75.5	0.135	0.0163
PK_{100}								
trans 1	31.2	63.3	0.0521	0.0785	15.8	48.2	0.1382	0.0874
trans 2	35.9	72.5	0.264	0.0591	64.4	82.2	0.148	0.0218
PK_{200}								
trans 1	34.9	67.9	0.0763	0.0801	18.1	53.3	0.139	0.0880
trans 2	41.2	76.6	0.237	0.0607	69.3	88.2	0.143	0.0246
PK_{1000}								
trans 1	36.4	77.4	0.0916	0.0760	25.3	62.0	0.119	0.0735
trans 2	48.0	82.2	0.188	0.0607	nd	nd	nd	nd

[a] Simultaneous fitting of sequential transitions to UV melting profiles taken at 260 and 280 nm was done as described in Materials and Methods. Units are kcal/mol for ΔH_{vH} and degrees Celsius for T_m. nd, transition temperature too high for parameters to be determined. [b] Buffers are 5 mM potassium phosphate plus the millimolar concentration of KCl indicated by the subscript.

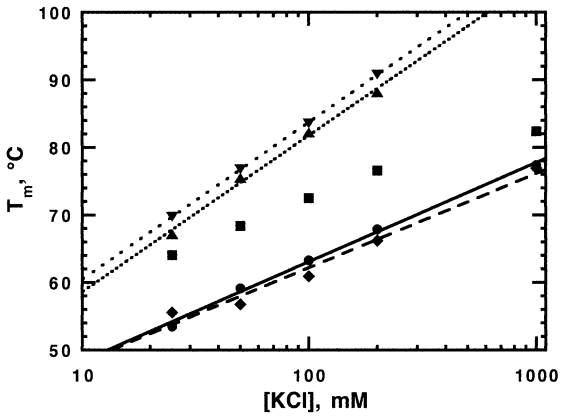

FIGURE 6: Summary of melting temperature salt dependence for G80, H1, and H2 RNAs: H1 RNA transition 1 (●), H1 RNA transition 2 (■), H2 RNA transition 2 (▲), G80 RNA transition 1 (◆), and G80 RNA transition 2 (▼). Lines fit to G80 RNA transition 1 and transition 2 have slopes of 14.7 and 23.5 deg, respectively.

pseudoknot structure to melt. The pseudoknot unfolding is consistently ~2° higher than the T_m of H2, for unknown reasons.

H1 RNA melts in a single, broad transition (Figure 5A), and at KCl concentrations of 200 mM or less the apparent T_m at 260 nm is lower than at 280 nm. Either melting in two steps with closely spaced T_ms or non-two-state unfolding (such as "fraying" of base pairs) could account for this behavior. We simply used two-wavelength analysis to obtain parameters for two transitions from these data (Table 2). The total van't Hoff enthalpy increases from 64 kcal/mol at 25 mM KCl to 84 kcal/mol at 1000 mM. The predicted nearest neighbor base pair stacking enthalpy for H1 is 78 kcal/mol, in good agreement with the van't Hoff enthalpy in higher salt. It is not possible to decide whether the H1 stem actually melts in two distinct steps or whether A-U pairs near the bulged A (which should have a larger hyperchromicity at 260 than the rest of the stem) tend to melt before the rest of the helix.

Since we have identified the second G80 RNA unfolding step with stem 2, melting of H1 RNA should be analogous to the first pseudoknot unfolding step. Although the same stem base pairs may be melting in each case, the context of the stem differs in the two RNAs: H1 has a hairpin loop where G80 RNA has stem 2 intact. Comparison of H1 RNA T_ms with those of the first G80 RNA transition shows that the stem is somewhat more stable in the pseudoknot (Figure 6), consistent with the H1 hairpin loop contributing a larger unfolding entropy. It is also noteworthy that H1 unfolding deviates from two-state behavior much more strongly than does the G80 RNA first unfolding step; in some way the pseudoknot context must promote cooperative unfolding of the stem.

Effects of Monovalent Ion Identity on Pseudoknot and Hairpin Stabilities. Increasing concentrations of monovalent ions stabilize duplex nucleic acids, and within group IA alkali metals, helix stability is only weakly sensitive to the ion type: smaller ions slightly decrease duplex DNA stability (Najah-Zadeh *et al*., 1995). Group IA ions have an opposite and much more dramatic effect on the stability of tRNA tertiary structure: the first unfolding transition of yeast $tRNA^{Phe}$ is 25° more stable in Li^+ than in Cs^+ (Urbanke *et al*., 1975; Heerschap *et al*., 1985). With these considerations in mind, we explored how monovalent ion type would affect the stability of G80 and H1 RNAs.

Example melting profiles of G80 and H1 RNAs in buffers with 200 mM LiCl or CsCl are shown in panels A and C of Figure 7. Melting profiles obtained in each of the group IA metal ions and NH_4^+ were analyzed in terms of two two-state unfolding transitions, and the T_ms are plotted in Figure 7B,D as a function of ionic radius. For G80 RNA, the T_m of the first unfolding step varies inversely with the ionic radius for the group IA ions, and NH_4^+ is more stabilizing than would be predicted on the basis of its size. The same qualitative trend in transition stability is observed for salt concentrations of 50 or 1000 mM as well (data not shown).

H1 RNA is also less stable in CsCl than in LiCl, though the differences between melting profiles in the two salts are not as large as for the G80 RNA first transition (Figure 7A,C). It is apparent that the overall cooperativity of H1 unfolding is higher in Li^+ than in Cs^+. When these melting profiles are analyzed in terms of two transitions, it is only the first transition that is affected by the ion identity (Figure 7D).

Effects of Divalent Ions on Pseudoknot Stability. Mg^{2+} is known to strongly favor pseudoknot formation, and in some cases a pseudoknot fold is adopted at moderate monovalent salt concentrations only if millimolar concentrations of Mg^{2+} are also present (Wyatt *et al*., 1990). A quantitative way to analyze the effects of Mg^{2+} on RNA stability is to plot $1/T_m$ vs $\log[Mg^{2+}]$; the slope of the resulting curve at a particular Mg^{2+} concentration is related to the number of ions released in the unfolding reaction, $\Delta\nu$, by

$$\Delta\nu = -\frac{\Delta H}{R}\frac{d(1/T_m)}{d\ln[Mg^{2+}]} \quad (4)$$

where ΔH is the enthalpy of the RNA unfolding transition and R is the gas constant. If an RNA has specific, high-affinity sites for Mg^{2+}, the plot may be linear to high ion concentrations; if there is only weaker, delocalized Mg^{2+} binding to both folded and unfolded forms of the RNA, $\Delta\nu$ will decrease at high ion concentrations and the plot will be

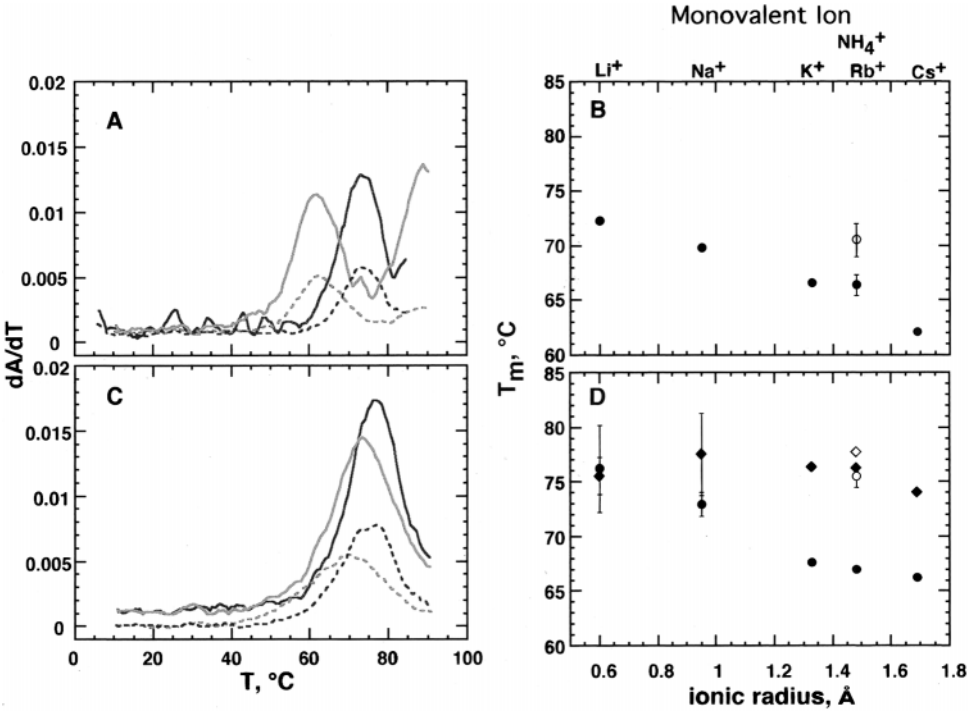

FIGURE 7: Monovalent ion type affects the thermal stability of G80 and hairpin I RNAs. (A) Melting profiles of G80 RNA determined in buffer with 200 mM monovalent salt: LiCl at 280 nm (black solid line) or 260 nm (black dashed line) and CsCl at 280 nm (red solid line) or 260 nm (red dashed line). (B) T_m versus ionic radius for G80 RNA (transition 1) in buffer with 200 mM monovalent salt: group IA ions (●) and NH_4^+ (○). (C) Melting profiles of H1 RNA determined in buffer with 200 mM monovalent salt: LiCl at 280 nm (black solid line) or 260 nm (black dashed line) and CsCl at 280 nm (red solid line) or 260 nm (red dashed line). (D) T_m versus ionic radius for H1 RNA in buffer with 200 mM monovalent salt: transition 1 T_m for group IA ions (●) and NH_4^+ (○); transition 2 T_m for group IA ions (◆) and NH_4^+ (◇).

curved (Laing *et al*., 1994). In one study of a pseudoknot, $1/T_m$ vs log[Mg^{2+}] was a straight line yielding $\Delta\nu \approx 1$, which was tentatively interpreted in terms of a single Mg^{2+} binding site within the pseudoknot (Qiu *et al*., 1996). We have examined the effects of various divalent ions on the stability of G80 RNA to see if we can find evidence for specific pseudoknot−Mg^{2+} interactions.

Figure 8A shows the effects of a 0.5 mM concentration of several divalent ions on the first unfolding step of G80 RNA in buffer containing 200 mM KCl. (A high salt concentration was chosen to promote two-state behavior in this transition.) Divalent ions differ in their effectiveness at stabilizing the pseuoknot: the order of stabilization is $Mn^{2+} > Mg^{2+} > Sr^{2+} \approx Ba^{2+} > Ca^{2+}$, over about a 2-fold range of free energy. Note that the trend among the group IIA ions does not correlate with ionic radius, as Ca^{2+} is slightly less effective than the larger Sr^{2+} and Ba^{2+}.

A plot of $1/T_m$ vs log[Mg^{2+}] for three of the ions is shown in Figure 8B. The apparent number of ions released is about 1 for Mn^{2+} and 1.4 for Mg^{2+} and Ba^{2+}. A problem with this analysis is that the high initial T_m of the pseudoknot in 200 mM KCl means that a relatively narrow range of divalent ion concentrations can be examined; to estimate the relative affinity of divalent ions for folded and unfolded forms of the pseudoknot, it is necessary to obtain T_ms at 10-fold higher ion concentrations.

To increase the accessible range of ion concentrations, we used urea to decrease the transition T_ms. The T_ms and van't Hoff enthalpies derived from G80 RNA melting profiles in increasing urea concentrations are plotted in panels A and B of Figure 9. The dependences of the T_ms on percentage urea are linear to within experimental error, and van't Hoff enthalpies decrease by only very small amounts. Similar linear behavior was obtained when $MgCl_2$ was included in the buffer, though the slopes change significantly between 0.1 and 1.0 mM $MgCl_2$ (Figure 9C). Linear extrapolation to 0% urea, using data taken between 10% and 50% urea, consistently underestimates T_ms and enthalpies by a small amount, <1%. These small differences suggest that there is slight curvature in the plots, but for our present purposes we have not tried to define this further. We conclude that urea simply shifts G80 RNA melting profiles to lower temperatures without altering the fundamental characteristics of the unfolding reaction.

In the presence of 50% urea, both G80 RNA unfolding transitions could be followed at divalent metal ion concentrations up to 30 mM (Figure 10A). Figure 10B plots $1/T_m$ of the first transition vs log[M^{2+}] for Mn^{2+}, Mg^{2+}, and Ba^{2+}. Above 5−10 mM M^{2+}, the slopes of the curves are clearly becoming less negative. These data were fit to a model that assumes (i) every phosphate is a potential M^{2+} binding site and (ii) ions interact nonspecifically with the RNA backbone with an excluded site size of two phosphates (eq 2 of Materials and Methods). The two variables in the model are the affinities of the ion for folded and unfolded states of the RNA. The curves shown in Figure 10 have been fit to this model using 16, the number of nucleotides in stem 1, as the number of phosphates; calculated binding affinities are given in Table 3. Doubling the number of phosphates involved in the unfolding reaction lowers the calculated M^{2+} binding constant for the folded form by about 25% and increases its affinity for the unfolded RNA by about the same amount, without significantly changing the quality of the fit. Lowering the number of phosphates below 12 results in

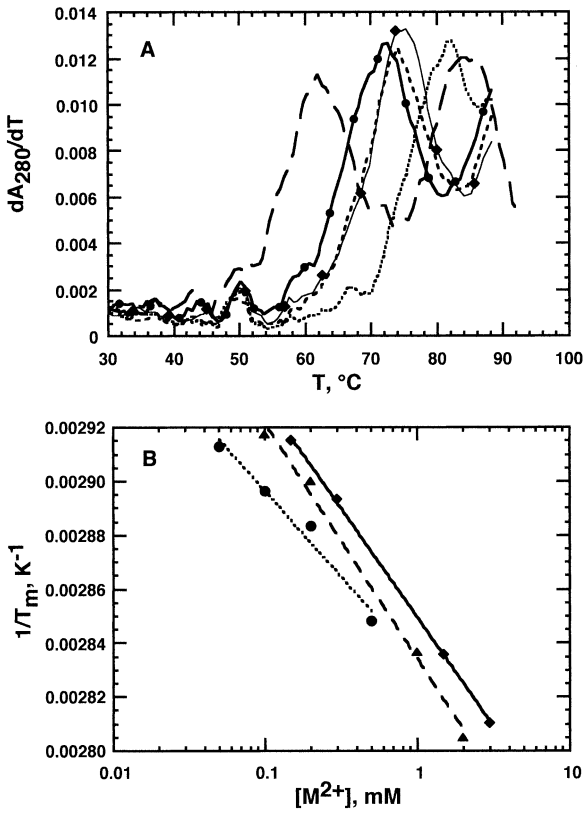

FIGURE 8: Divalent ions stabilize G80 RNA. (A) Melting profiles of G80 RNA in buffer with 200 mM KCl (—) and 200 mM KCl and 0.5 mM $BaCl_2$ (◆), $CaCl_2$ (●), $SrCl_2$ (– –), or $MnCl_2$ (---). (B) $1/T_m$ as a function of log $[M^{2+}]$ for G80 RNA transition 1 in 200 mM KCl and different divalent ions. Using ΔH_{vH} = 65 kcal/mol, $\Delta\nu$ calculated using eq 3 is 1.3 for $BaCl_2$ (◆), 1.41 for $MgCl_2$ (▲), and 1.03 for $MnCl_2$ (●).

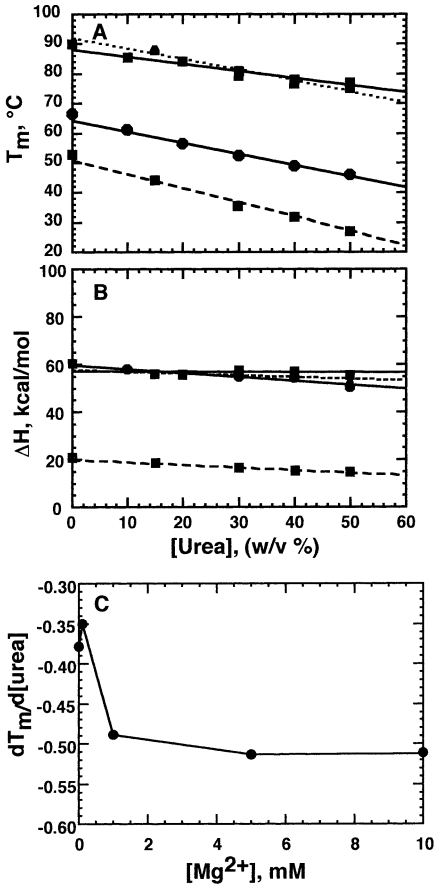

FIGURE 9: Increasing urea concentrations destabilize G80 and H2 RNAs. Melting experiments were carried out in buffer with 200 mM KCl. (A) Dependence of transition T_m on urea concentration (w/v) for G80 RNA and H2 RNAs. G80 RNA: transition 1 (—⬣—) and transition 2 (—■—). H2 RNA: transition 1 (--■--) and transition 2 (--▲--). Least squares fits of lines excluded the points at 0 urea. (B) Dependence of ΔH_{vH} on urea concentration for G80 RNA and H2 RNAs. G80 RNA: transition 1 (—⬣—) and transition 2 (—■—). H2 RNA: transition 1 (--■--) and transition 2 (--▲--). Least squares fits of lines excluded the points at 0 urea. (C) Dependence of G80 RNA transition 1 T_m on urea concentration at different $MgCl_2$ concentrations (with 200 mM KCl). The ranges of urea concentrations used to find d(T_m)/d[urea] were 0 Mg^{2+}, 5−50%; 0.1−5 mM Mg^{2+}, 10−50%; 10 mM Mg^{2+}, 20−50%.

poorer fits. In particular, curves generated with the assumption that there is one ion binding site with different affinities in the folded and partially unfolded intermediate forms cannot account for the data. Curved plots of $1/T_m$ vs log$[M^{2+}]$ were also obtained for the second G80 RNA unfolding step (Figure 10C). (Data for Mn^{2+} were unreliable due to significant RNA hydrolysis at high temperatures.) The estimated M^{2+} affinities for the completely unfolded RNA are weaker than those for the folded and intermediate forms, as expected (Table 3).

As a check of the effects of urea on Mg^{2+}−RNA interactions, the Mg^{2+} dependence of the T_m for transition 1 has been extrapolated to 0% urea using the data of Figure 9C. These extrapolated points are plotted in Figure 10D and correspond well to the data in Figure 8B for points below 2 mM Mg^{2+}. The calculated Mg^{2+} affinities are 2−3-fold higher after extrapolation, but the difference in affinities between fully folded and partially unfolded pseudoknot is still relatively small (Table 3).

DISCUSSION

Pseudoknot Unfolding Energetics. In the present work, both UV hyperchromicity and calorimetry were used to follow G80 RNA unfolding. UV melting experiments are useful for scanning a large number of buffer conditions with a moderate amount of material and can be analyzed to yield van't Hoff enthalpies for a minimum number of transitions. Two-wavelength analysis considerably improves the reliability of the approach by allowing closely spaced transitions to be resolved, but the technique may still seriously underestimate the number of unfolding transitions and the total enthalpy of unfolding. Scanning calorimetry in principle provides a direct measure of the unfolding enthalpy, though in practice errors can arise because of RNA hydrolysis and uncertainties in interpolating a baseline between high and low temperatures. A combination of UV and calorimetry experiments is a more reliable way to analyze multistate RNA melting data than either approach alone, especially if a wide range of buffer conditions can be examined (Draper & Gluick, 1995).

We have obtained a consistent picture of the pathway and energetics of G80 RNA unfolding by combining melting data from UV hyperchromicity and calorimetry experiments on the intact pseudoknot and its component hairpins at different salt concentrations. Stem 1 melts before stem 2, and the total enthalpy of unfolding is approximately independent of salt concentration. However, unfolding deviates strongly from two-state behavior at low salt concentrations, and only at fairly high salt concentrations (≥200 mM) are two-state

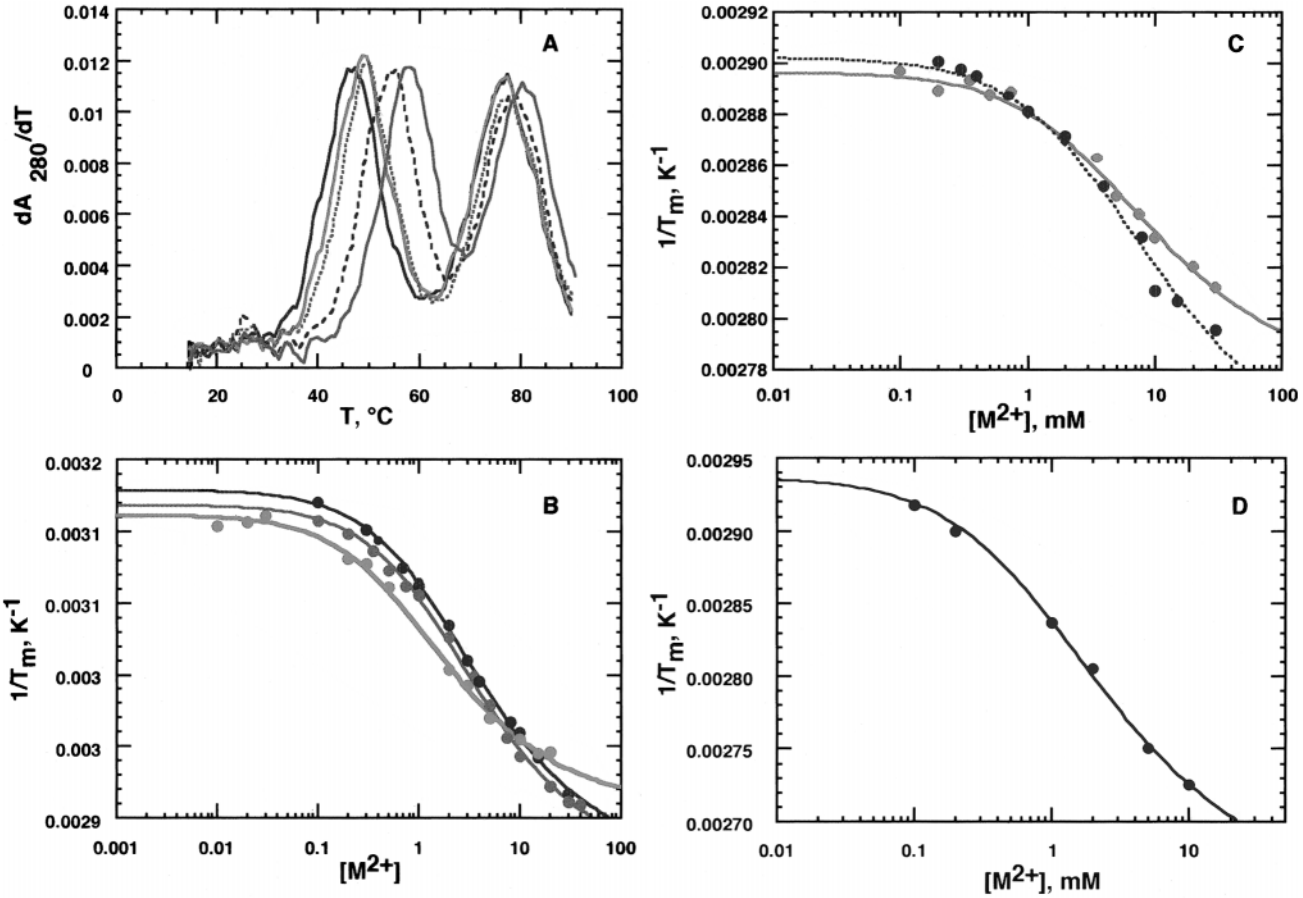

FIGURE 10: Binding of divalent ions to G80 RNA. (A) Melting profiles of G80 RNA in buffer with 200 mM KCl, 50% urea, and 0 (black), 0.1 mM (red), 0.2 mM (dashed green), 1 mM (dashed black), or 2 mM (green) $MgCl_2$. (B) Dependence of $1/T_m$ of transition 1 on log $[M^{2+}]$ for several divalent ions: $BaCl_2$ (black), $MgCl_2$ (green), and $MnCl_2$ (red). Buffer conditions are as in panel A. (C) Plot of $[M^{2+}]$ versus $1/T_m$ for G80 RNA transition 2, using conditions as in panel B: Mg^{2+} (red) and Ba^{2+} (black). (D) Extrapolation of G80 RNA transition 1 T_ms to 0% urea using slopes in Figure 9C. Solid lines in panels B, C, and D are fits to eq 2 with $m = 16$; binding constants are listed in Table 3.

Table 3: RNA Binding Affinities of Divalent Ions[a]

RNA	$[M^+]$	Mg^{2+}	Ba^{2+}	Mn^{2+}
G80 RNA, trans 1	0.2 M, 50% urea	300	300	580
		130	120	290
	0.2 M, 0% urea[b]	710		
		220		
G80 RNA, trans 2	0.2 M, 50% urea	160	120	nd[c]
		90	60	nd[c]
72 RNA[d]	0.1 M	480		
		260		
poly(A)−poly$(U)_2$[e]	0.2 M	230		
poly(A)−poly(U)[e]	0.2 M	150		
poly(A)[e]	0.2 M	140		
poly(U)[e]	0.2 M	80		

[a] The two constants reported for G80 RNA transitions and for 72 RNA are ion affinities for folded and unfolded forms of the RNA, obtained by analysis of the ion dependence of melting temperatures as described in the text. Errors are about ±15% for determinations in 50% urea and ±25% for the extrapolation to 0% urea. Other data were obtained by direct measurement of binding isotherms as noted in cited references. Binding constants are M^{-1}. [b] Binding affinities extrapolated to 0% urea. [c] Not determined; hydrolysis was too severe at high concentrations of Mn^{2+}. [d] Data taken from Laing *et al*., 1994. [e] Extrapolated from data taken at lower salt concentrations (Record *et al*., 1976) using the data of Krakauer (1971).

transitions adequate models for the unfolding. The total enthalpy of unfolding, ~170 kcal/mol, is approximately the quantity expected from nearest neighbor base stacking of stem base pairs and adjacent nucleotides, and it is not neceesary to postulate additional interactions beyond the secondary structure diagrammed in Figure 1.

Unfolding thermodynamics of two other pseudoknot sequences have been studied. One is a model sequence with stems of three and five base pairs; it is relatively unstable and forms a hairpin structure unless buffers contain 0.5 M NaCl or millimolar concentrations of Mg^{2+} (Wyatt *et al*., 1990). The other pseudoknot is a structure from T4 gene 32 mRNA and is thought to be a recognition site for gene 32 protein. With stems of four and seven base pairs, it is more stable than the model pseudoknot and forms in 50 mM NaCl in the absence of Mg^{2+} (Qiu *et al*., 1996). Both pseudoknots apparently melt in a single unfolding step, with van't Hoff enthalpies only 65−75% of those predicted from base pair stacking enthalpies alone. For the model pseudoknot sequence, this discrepancy was interpreted as a distortion of helix structure that reduced base stacking in the completely folded molecule (Puglisi *et al*., 1991). On the basis of our findings with G80 RNA, it seems more likely that these two pseudoknots actually unfold in two closely spaced transitions and that two-state analysis has underestimated the total unfolding enthalpy.

Monovalent Ions and Pseudoknot Stability. The negative charge of long polynucleotides is partially neutralized by accumulated counterions, whose concentration near the nucleic acid surface is approximately independent of the solution salt concentration. Counterion condensation theory

predicts a simple relation between linear charge density of the polynucleotide and the fraction of a counterion bound per nucleotide phosphate (Manning, 1978). The salt dependence of the T_m of a polynucleotide is a measure of the number of ions released in the unfolding; this number, in turn, reflects the difference in charge density between the two forms (Record, 1975). In DNA oligomers, end effects decrease the extent of ion binding, and the dependence of the melting temperature on salt concentration becomes less steep (Elson *et al*., 1970). However, the salt dependence of the T_m still reflects the difference in charge density between duplex and single-stranded oligomers.

The data in Figure 6 show that pseudoknot stem 1 unfolding is only 60% as sensitive to salt concentration as stem 2, even though the two stems have about the same unfolding enthalpies and number of nucleotides. For comparison, the number of ions released per phosphate for triple-helical poly(A)-poly$(U)_2$ melting to a duplex and single strand is only ~70% of the value for poly(A)-poly(U) melting (Manning, 1978). This suggests a rough correspondence between charge densities in the unfolding series pseudoknot → intermediate (stem 1 unfolded, stem 2 intact) → single strand and the series triplex → duplex + single strand → single strand. In principle, model calculations of the sort used by Olmsted and Hagerman (1994) to calculate the excess ion accumulation near a DNA four-helix junction could be used to quantitatively estimate the salt dependence of pseudoknot unfolding transitions.

The size of group IA metal ions has little effect on the extent of their binding to DNA. In an NMR study of the competition between different ions, the order of binding affinities was $Cs^+ > K^+ > Li^+ > Na^+$, but the largest difference in affinities was less than a factor of 2 (Bleam *et al*., 1980). This insensitivity to ionic radius is consistent with these ions remaining fully hydrated when bound to DNA. Similarly, the variation in poly[d(A-T)] T_m among equal concentrations of NaCl, KCl, and CsCl was less than 1.5° (Najah-Zadeh *et al*., 1995). Thus it was unexpected that G80 and H1 RNAs would show a distinct preference for small ions over larger ones (Figure 7).

A similar size-based discrimination among group IA ions is seen in some ion-specific glass electrodes (which are essentially cation exchangers) and membrane ion channel proteins. Eisenman has qualitatively explained this kind of selectivity as a balance between an unfavorable free energy of ion dehydration and a favorable Coulombic energy. These two factors depend on ion radius in opposite ways: dehydration is energetically more costly for smaller ions, but smaller ions can also approach negative charges more closely and recover a larger electrostatic free energy (Eisenman, 1962; Eisenman & Horn, 1983). Thus ion binding affinity is expected to be inversely proportional to radius in a "high-field" environment where (i) ions are at least partially dehydrated and (ii) there is a high density of negative charges. Conversely, Cs^+ will be preferred over Li^+ in a dehydrating environment with low charge density, where the cost of dehydration is not as strongly offset by electrostatic interactions. This idea has been invoked to interpret the preference of G-quadruplex structures for binding K^+ over Na^+ in the dehydrated channel formed by guanosine bases (Hud *et al*., 1996).

The trend we observed for H1 and G80 RNA stabilization by alkali metal ions would be explained, according to Eisenman's proposal, if monovalent ions are partially dehydrated and in a high charge density environment when bound to these RNAs. The spacing of negative charges in a double helix is too large for an ion to interact with more than one phosphate at a time, and, as pointed out above, a helix consequently does not discriminate among different size ions. But conceivably the bulged A or hairpin loop of H1 could create a higher charge density that favors binding of small ions, and preferential ion binding in these regions might enhance two-state melting behavior. In the pseudoknot, loop 1 and loop 2 cross stem grooves and possibly create regions of unusually high charge density that selectively bind smaller ions. Whether monovalent cations are actually dehydrated to some degree when bound to the pseudoknot will require further work to substantiate. However, it is notable that tRNA tertiary structure shows the same selectivity for small ions as G80 RNA, but with a more dramatic 25° difference in stability between Li^+ and Cs^+ (Urbanke *et al*., 1975; Heerschap *et al*., 1985). A ribosomal RNA tertiary structure is selective for NH_4^+ and K^+ over other ions (Wang *et al*., 1993). It may be that monovalent ion selectivity is a common feature of the high charge densities created by RNA tertiary structures.

Divalent Ions and Pseudoknot Stability. Mg^{2+} and other closed shell alkaline earth cations are thought to interact with DNA as hydrated ions in an entirely delocalized fashion (Skerjanc & Strauss, 1968; Manning, 1977), and no site-bound interactions of these ions with duplex DNA can be detected by Raman spectroscopy (Duguid *et al*., 1995). But the irregular structure of an RNA can clearly create sites capable of chelating metal ions, as observed in RNA crystal structures (see introduction). We were interested to know whether the known sensitivity of pseudoknot folding to Mg^{2+} is a consequence of site-specific interactions, perhaps near the helix junction as proposed by others (Puglisi *et al*., 1990), or whether delocalized binding can account for pseudoknot stability in the presence of Mg^{2+}.

The melting experiments presented here sense only those divalent ions released upon unfolding of the pseudoknot structure. Thus the binding constants listed for G80 RNA in Table 3 do not necessarily refer to all the ions bound to the RNA (as would be observed by equilibrium dialysis or other measure of a binding isotherm) but only those whose affinities alter upon RNA unfolding. In considering the thermodynamic contributions of divalent ions to pseudoknot stability, it is precisely this group of released ions whose affinities are needed. Unfortunately, melting experiments cannot easily resolve classes of ions with different binding affinities: constants in Table 3 are average affinities for all the ions released in an unfolding step. Hence the problem arises of how to distinguish any site-specific interactions from the expected background of delocalized, nonspecific interactions. Toward a resolution of this problem, Table 3 also lists Mg^{2+}−RNA binding constants measured for homopolymers and a hairpin, for comparison to G80 RNA ion affinities, and we offer several comments:

(i) Delocalized binding cannot be ignored in considering the stability of the pseudoknot. Stem 2 of G80 RNA provides an internal control, in that its structure at high temperature is simply a helix and single strands; no special

Mg^{2+} binding pockets are expected. Yet its stability is clearly sensitive to divalent ion concentrations in the same concentration range as the intact pseudoknot. Mg^{2+} affinity for duplex RNA is weak, but it can be calculated from the affinities in Table 3 (using eq 3 in Materials and Methods) that the number of Mg ions electrostatically bound to a 16-nucleotide segment of duplex RNA (the length of stem 1) in 0.2 M monovalent salt is about 1.7, and about 0.4 of these are released upon melting of the duplex to single strands. This number of released Mg ions is of the same order as the 1.4 ions measured for melting of the pseudoknot stem 1. Although a 16-nucleotide duplex will behave somewhat differently in the contexts of a pseudoknot or long polymer, this rough calculation suggests that the number of Mg ions released in pseudoknot melting must contain a significant contribution from nonspecifically bound ions.

(ii) The pseudoknot appears to bind divalent ions more tightly (on average) than hairpin or duplex RNA. Even in the presence of urea, the average affinity of ions for the folded pseudoknot is about twice as large as for poly(A)-poly(U), and the value extrapolated to 0% urea is about 5-fold larger than for duplex and 3-fold larger than for triplex RNAs. This suggests that there is a region with a higher charge density than triplex RNA or that there are specific chelation site(s). Equation 2 can be modified to take into account two classes of binding sites, by substitution of

$$(0.5 + 0.5(1 + 4K_1L)^{1/2})^n(0.5 + 0.5(1 + 4K_2L)^{1/2})^{(m-n)} \quad (5)$$

in the numerator of the log term. There is no unique set of K_1, K_2, and n values for the Figure 10 data, of course, but this equation can be used to estimate an upper limit on ion affinity for a class of n sites. For instance, if five potential tight sites are assumed, the binding data in the absence of urea (Figure 10D) can be fit with K_1 as large as 2×10^3 M^{-1}. In this case, the 11 remaining weak sites bind with an affinity of 240 M^{-1}, and binding to the partially unfolded pseudoknot is 140 M^{-1}. The latter two affinities are reasonable for nonspecific Mg^{2+} binding to folded and partially unfolded forms (compare homopolymer affinities for Mg^{2+} in Table 3). If fewer and tighter sites are assumed (e.g., for $n = 2$, K_1 is a maximum of 5×10^3 M^{-1}), then the remaining weak sites are much stronger than expected for nonspecific binding to duplex or triplex RNA ($K_2 = 370$ M^{-1}).

(iii) The weak selectivity of the pseudoknot for divalent ions suggests that there is only a small site-specific component in its interactions with ions. As discussed for monovalent ions, delocalized binding of divalent ions should be essentially independent of ionic radius. The range of pseudoknot stabilities seen in Figure 8A with different divalent ions is therefore suggestive of some localized interactions. However, these small T_m differences can be caused by only slight (less than 2-fold) differences in ion binding affinities (Table 3). For comparison, two high-affinity ion sites in a ribosomal RNA fragment show 10−50-fold discrimination between Mg^{2+}, Ca^{2+}, and Ba^{2+} (Bukhman & Draper, 1997). Thus divalent ions are probably not extensively coordinated to the pseudoknot. [Mn^{2+} is known to bind to N7 of DNA purines under conditions where similar interactions of alkaline earth cations cannot be detected (Duguid *et al*., 1995), which may account for its higher affinity for both folded and unfolded RNA.]

On the basis of the affinities and weak selectivity of G80 RNA for divalent ions, we suggest that the pseudoknot has a limited region (perhaps five phosphates) that (i) binds divalent ions with higher affinity than expected for a regular duplex and (ii) makes some direct contacts with ions. The junction of the two helices is an obvious location for such site(s), and Puglisi *et al*. (1990), in an NMR study of a model pseudoknot, have pointed out a close juxtaposition of loop phosphates that would create both a high electrostatic field and the opportunity for weak ion chelation by direct contacts. The junction might be considered an "intermediate" ion binding region, containing several "sites" in between highly ligated specific sites and purely delocalized binding in character. Strong electrostatic interactions and few direct RNA contacts should enhance the ion binding affinity over delocalized ions but yield only weak selectivity based on ion size.

There are few RNAs for which crystallographic and thermodynamic studies of divalent metal ions binding can be correlated. Of some relevance as a potential "intermediate" ion binding site is the U-turn fold conserved in hammerhead ribozymes and tRNA anticodon loops. It is known to bind Mg^{2+} or Pb^{2+} by coordination to one phosphate and hydrogen bonding via water to two or three bases (Holbrook *et al*., 1975; Brown *et al*., 1985; Scott *et al*., 1995), has an affinity of $(1-2) \times 10^3$ M^{-1} for Mg^{2+} in 0.14 M monovalent salt, and discriminates only weakly between different divalent ions (Labuda & Pörschke, 1982; Bujalowski *et al*., 1986; Menger *et al*., 1996). It is an order of magnitude weaker in affinity than the strongest Mg^{2+} binding site in tRNA (Stein & Crothers, 1976), which is probably more deeply buried within the tRNA structure between the D and TψC loops (Jack *et al*., 1977; Draper, 1985).

It is instructive to compare the relative contributions to pseudoknot stability of intermediate sites vs nonspecific, delocalized sites. Using the maximum affinity estimated in (ii) above for five stronger sites, calculations show that the free energies of binding the stronger and weaker classes of ions are nearly equal over the concentration range 1−10 mM Mg^{2+}. This estimate underscores the importance of nonspecific ion binding in the stabilization of RNA structures. Calculations by Olmsted and Hagerman (1994) on four-branch DNA molecules suggested that a significant excess of counterions accumulates in the junction region, relative to linear DNA. They pointed out that junction stability should therefore show increased sensitivity to monovalent salt concentrations and that positively charged ligands (such as Mg^{2+}) should preferentially bind near the junction. The high charge densities that develop within RNA tertiary structures must similarly accumulate a dense cation atmosphere, and the unusual sensitivity of RNA folding to ionic conditions may be in large part due to interactions with delocalized ions.

ACKNOWLEDGMENT

We thank the Johns Hopkins Biocalorimetry Center for help with preliminary experiments and Dr. Dong Xie of SAIS, Frederick, MD, for the use of the calorimeter.

REFERENCES

Anderson, C. F., & Record, M. T., Jr. (1995) Salt−Nucleic Acid Interactions, *Annu. Rev. Phys. Chem. 46*, 657−700.

Bina-Stein, M., & Stein, A. (1976) Allosteric Interpretation of Mg^{2+} Binding to the Denaturable *Escherichia coli* $tRNA^{Glu_2}$, *Biochemistry 15*, 3912−3917.

Bleam, M. L., Anderson, C. F., & Record, M. T., Jr. (1980) Relative binding affinities of monovalent cations for double-stranded DNA, *Proc. Natl. Acad. Sci. U.S.A. 77*, 3085−3089.

Breslauer, K. J., Sturtevant, J. M., & Tinoco, I., Jr. (1975) Calorimetric and Spectroscopic Investigation of the Helix-to-Coil Transition of a Ribooligonucleotide: rA_7U_7, *Biochemistry 14*, 549−565.

Brown, R. S., Dewan, J. C., & Klug, A. (1985) Crystallographic and Biochemical Investigation of the Lead(II)-Catalyzed Hydrolysis of Yeast Phenylalanine tRNA, *Biochemistry 24*, 4785−4801.

Bujalowski, W., Graeser, E., McLaughlin, L. W., & Pörschke, D. (1986) Anticodon Loop of $tRNA^{phe}$: Structure, Dynamics, and Mg^{2+} Binding, *Biochemistry 25*, 6365−6371.

Bukhman, Y. V., & Draper, D. E. (1997) Affinities and Selectivities of Divalent Cation Binding Sites Within an RNA Tertiary Structure, *J. Mol. Biol. 273*, 1020−1031.

Cate, J. H., Gooding, A. R., Podell, E., Zhou, K., Golden, B. L., Kundrot, C. E., Cech, T. R., & Doudna, J. A. (1996) Crystal structure of a group I ribozyme domain: principles of RNA packing, *Science 273*, 1678−1685.

Chen, X., Kang, H., Shen, L. X., Chamorro, M., Varmus, H. E., & Tinoco, I., Jr. (1996) A Characteristic Bent Conformation of RNA Pseudoknots Promotes −1 Frameshifting during Translation of Retroviral RNA, *J. Mol. Biol. 260*, 479−483.

Draper, D. E. (1985) On the Coordination Properties of Eu^{3+} Bound to tRNA, *Biophys. Chem. 21*, 91−101.

Draper, D. E., & Gluick, T. C. (1995) Melting Studies of RNA Unfolding and RNA−Ligand Interactions, in *Energetics of Biological Macromolecules* (Johnson, M. L., & Ackers, G., Eds.) pp 281−305, Academic Press, San Diego.

Duguid, J. G., Bloomfield, V. A., Benevides, J. M., & Thomas, G. J. (1995) Raman Spectroscopy of DNA−Metal Complexes. II. The Thermal Denaturation of DNA in the Presence of Sr^{2+}, Ba^{2+}, Ca^{2+}, Mn^{2+}, Co^{2+}, Ni^{2+}, and Cd^{2+}, *Biophys. J. 69*, 2623−2641.

Eisenman, G. (1962) Cation selective glass electrodes and their mode of operation, *Biophys. J. 2*, 259−323.

Eisenman, G., & Horn, R. (1983) Ionic Selectivity Revisited: The Role of Kinetic and Equilibrium Processes in Ion Permeation Through Channels, *J. Membr. Biol. 76*, 197−225.

Elson, E. L., Scheffler, I. E., & Baldwin, R. L. (1970) Helix formation by d(TA) oligomers. III. Electrostatic effects, *J. Mol. Biol. 54*, 401−415.

Gluick, T. C., & Draper, D. E. (1994) Thermodynamics of Folding a Pseudoknotted mRNA Fragment, *J. Mol. Biol. 241*, 246−262.

Gluick, T. C., Gerstner, R. G., & Draper, D. E. (1997) Effects of Mg^{2+}, K^+, and H^+ on an equilibrium between alternative conformations of an RNA pseudoknot, *J. Mol. Biol. 241*, 401−415.

Heerschap, A., Walters, J. A. L. I., & Hilbers, C. W. (1985) Interactions of some naturally occurring cations with phenylalanine and initiator tRNA from yeast as reflected by their thermal stability, *Biophys. Chem. 22*, 205−217.

Hill, T. L. (1957) Some Statistical Problems Concerning Linear Macromolecules, *J. Polym. Sci. 23*, 549−562.

Holbrook, S. R., Sussman, J. L., Warrant, R. W., Church, G. M., & Kim, S.-H. (1977) RNA−ligand interactions: magnesium binding sites in yeast $tRNA^{Phe}$, *Nucleic Acids Res. 4*, 2811−2820.

Hud, N. V., Smith, F. W., Anet, F. A., & Feigon, J. (1996) The selectivity for K^+ versus Na^+ in DNA quadruplexes is dominated by relative free energies of hydration: a thermodynamic analysis by ^1H NMR, *Biochemistry 35*, 15383−15390.

Jack, A., Ladner, J. E., Rhodes, D., Brown, R. S., & Klug, A. (1977) A Crystallographic Study of Metal-Binding to Yeast Phenylalanine Transfer RNA, *J. Mol. Biol. 111*, 315−328.

Krakauer, H. (1971) The Binding of Mg^{++} Ions to Polyadenylate, Polyuridylate, and Their Complexes, *Biopolymers 10*, 2459−2490.

Krakauer, H. (1974) A Thermodynamic Analysis of the Influence of Simple Mono- and Divalent Cations on the Conformational Transitions of Polynucleotide Complexes, *Biochemistry 13*, 2579−2589.

Labuda, D., & Pörschke, D. (1982) Magnesium Ion Inner Sphere Complex in the Anticodon Loop of Phenylalanine Transfer Ribonucleic Acid, *Biochemistry 21*, 49−53.

Laggerbauer, B., Murphy, F. L., & Cech, T. R. (1994) Two major tertiary folding transitions of the *Tetrahymena* catalytic RNA, *EMBO J. 13*, 2669−2676.

Laing, L. G., & Draper, D. E. (1994) Thermodynamics of RNA Folding in a Highly Conserved Ribosomal RNA Domain, *J. Mol. Biol. 237*, 560−576.

Laing, L. G., Gluick, T. C., & Draper, D. E. (1994) Stabilization of RNA Structure by Mg^{2+} Ion: Specific and Non-specific Effects, *J. Mol. Biol. 237*, 577−587.

Larsen, B., Gesteland, R. F., & Atkins, J. F. (1997) Structural probing and mutagenic analysis of the stem-loop required for *E. coli* dnaX ribosomal frameshifting: programmed efficiency of 50%, *J. Mol. Biol.* (in press).

Lowman, H. B., & Draper, D. E. (1986) On the Recognition of Helical RNA by Cobra Venom V_1 Nuclease, *J. Biol. Chem. 261*, 5396−5403.

Manning, G. S. (1977) Theory of the Delocalized Binding of Mg(II) to DNA: Preliminary Analysis for Low Binding Levels, *Biophys. Chem. 7*, 141−145.

Manning, G. S. (1978) The molecular theory of polyelectrolyte solutions with applications to the electrostatic properties of polynucleotides, *Q. Rev. Biophys. 11*, 179−246.

Najah-Zadeh, R., Wu, J. Q., & MacGregor, R. B. (1995) Effect of cations on the volume of the helix-coil transition of poly[d(A-T)], *Biochim. Biophys. Acta 1262*, 52−58.

Olmsted, M. C., & Hagerman, P. J. (1994) Excess Counterion Accumulation around Branched Nucleic Acids, *J. Mol. Biol. 243*, 919−929.

Puglisi, J. D., & Tinoco, I., Jr. (1989) Absorbance Melting Curves of RNA, *Methods Enzymol. 180*, 304.

Puglisi, J. D., Wyatt, J. R., & Tinoco, I., Jr. (1990) Conformation of an RNA Pseudoknot, *J. Mol. Biol. 214*, 437−453.

Puglisi, J. D., Wyatt, J. R., & Tinoco, I., Jr. (1991) RNA Pseudoknots, *Acc. Chem. Res. 24*, 152−158.

Qiu, H., Kaluarachchi, K., Dhu, Z., Hoffman, D. W., & Giedroc, D. P. (1996) Thermodynamics of Folding of the RNA Pseudoknot of the T4 Gene 32 Autoregulatory Messenger RNA, *Biochemistry 35*, 4176−4186.

Record, M. T., Jr. (1975) Effects of Na^+ and Mg^{++} Ions on the Helix-Coil Transition of DNA, *Biopolymers 14*, 2137−2158.

Record, M. T., Lohman, T. M., & de Haseth, P. (1976) Ion Effects on Ligand-Nucleic Acid Interactions, *J. Mol. Biol. 107*, 145−158.

Römer, R., & Hach, R. (1975) tRNA Conformation and Magnesium Binding, *Eur. J. Biochem. 55*, 271−284.

Scott, W. G., Finch, J. T., & Klug, A. (1995) The Crystal Structure of an All-RNA Hammerhead Ribozyme: A Proposed Mechanism for RNA Catalytic Cleavage, *Cell 81*, 991−1002.

Skerjanc, J., & Strauss, U. P. (1968) Interactions of Polyelectrolytes with Simple Electrolytes. III. The Binding of Magnesium Ion by Deoxyribonucleic Acid, *J. Am. Chem. Soc. 90*, 3201−3205.

Stein, A., & Crothers, D. M. (1976a) Conformational Changes of Transfer RNA. The Role of Magnesium(II), *Biochemistry 15*, 160−167.

Stein, A., & Crothers, D. M. (1976b) Equilibrium Binding of Magnesium(II) by *Escherichia coli* $tRNA^{fMet}$, *Biochemistry 15*, 157−160.

ten Dam, E., Pleij, K., & Draper, D. E. (1992) Structural and Functional Aspects of RNA Pseudoknots, *Biochemistry 31*, 11665−11676.

Turner, D. H., Sugimoto, N., & Freier, S. M. (1988) RNA Structure Prediction, *Annu. Rev. Biophys. Biophys. Chem. 17*, 167−192.

Urbanke, C., Römer, R., & Maas, G. (1975) Tertiary Structure of $tRNA^{Phe}$ (Yeast): Kinetics and Electrostatic Repulsion, *Eur. J. Biochem. 55*, 439−444.

Wang, Y.-X., Lu, M., & Draper, D. E. (1993) Specific Ammonium Ion Requirement for Functional Ribosomal RNA Tertiary Structure, *Biochemistry 32*, 12279−12282.

Williams, A. P., Longfellow, C. E., Freier, S. M., Kierzek, R., & Turner, D. H. (1985) Laser Temperature-Jump, Spectroscopic, and Thermodynamic Study of Salt Effects on Duplex Formation by dGCATGC, *Biochemistry 24*, 4283−4291.

Wills, N. M., Gesteland, R. F., & Atkins, J. F. (1991) Evidence that a downstream pseudoknot is required for translational read-through of the Moloney murine leukemia virus *gag* stop codon, *Proc. Natl. Acad. Sci. U.S.A. 88*, 6991−6995.

Wills, N. M., Gesteland, R. F., & Atkins, J. F. (1994) Pseudoknot-dependent read-through of retroviral gag termination codons: importance of sequences in the spacer and loop 2, *EMBO J. 13*, 4137−4144.

Wyatt, J. A., Puglisi, J. D., & Tinoco, I., Jr. (1990) RNA Pseudoknots. Stability and Loop Size Requirements, *J. Mol. Biol. 214*, 455−470.

Wyman, J., & Gill, S. (1990) *Binding and Linkage. Functional Chemistry of Biological Macromolecules*, University Science Books, Mill Valley, CA.

Zarrinkar, P. P., & Williamson, J. R. (1994) Kinetic Intermediates in RNA Folding, *Science 265*, 918−924.

BI971362V